ESP5403 Nanomaterials for Energy Systems

Size Effect on Transport Phenomena

Palani Balaya
mpepb@nus.edu.sg
6516 7644

Recall- Schottky barrier

Schottky barrier is formed between a metal and a *n* - or *p* - semiconductor when are brought into contact, such that
$\Phi_m > \Phi_s$

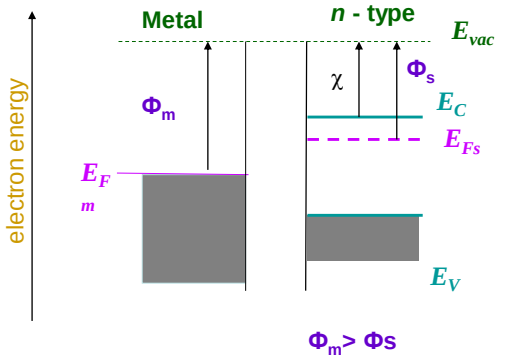

Energy band diagram of the metal and the semiconductor in isolation

Recall - Schottky barrier (in dark)

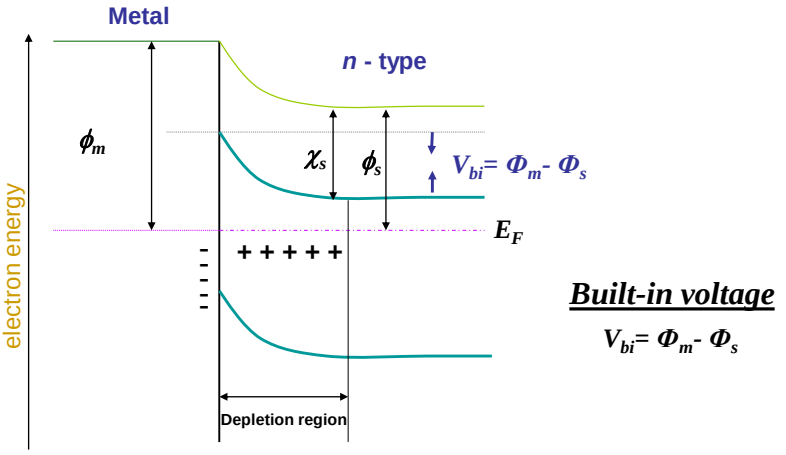

Energy band diagram of a metal-semiconductor contact in thermal equilibrium, in the dark

Concentration profile at Schottky barrier

Concentration profile

$$n = N_c e^{-(E_c - E_F)/k_B T}$$
$$p = N_v e^{-(E_F - E_v)/k_B T}$$

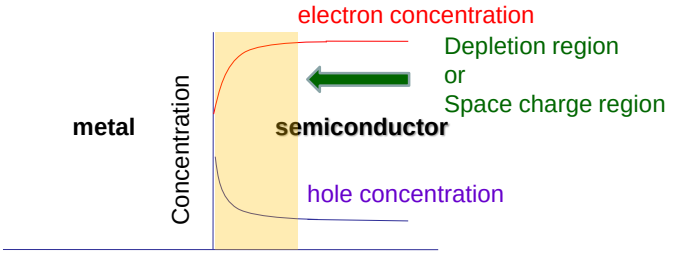

By joining metal and semiconductor we set up an electric field in a layer close to interface

Electric field will drive electrons and holes in opposite direction – separation

Contacts presents a lower resistance path for holes than electrons – from semiconductor to metals – this type of junction is an example for Schottky barrier

Schematic representation of bi-crystal

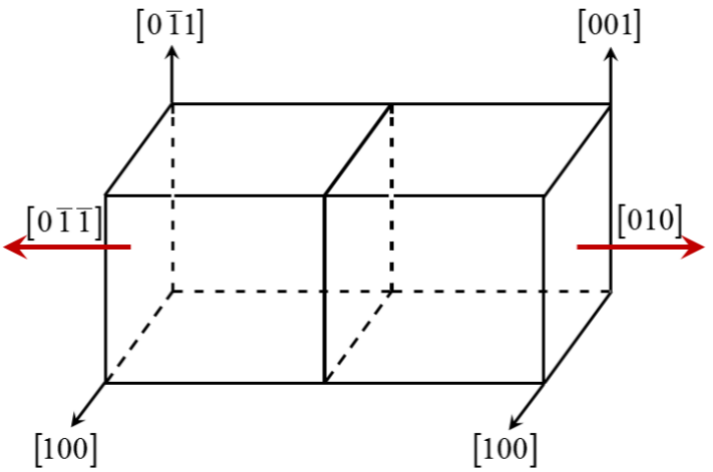

Grain boundary core – space charge model (Mott-Schokky)

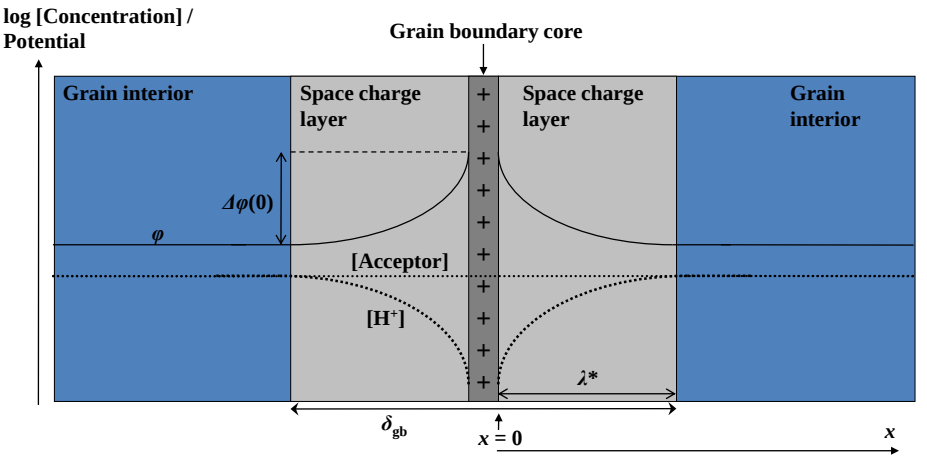

$\Delta\varphi(0)$ schottky barrier height δ_{gb} grain boundary width λ^* space charge layer width

Grain boundary core – space charge model

Example: Oxygen ion conductor (Y_2O_3 doped ZrO_2)

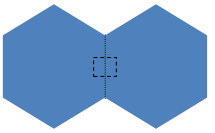

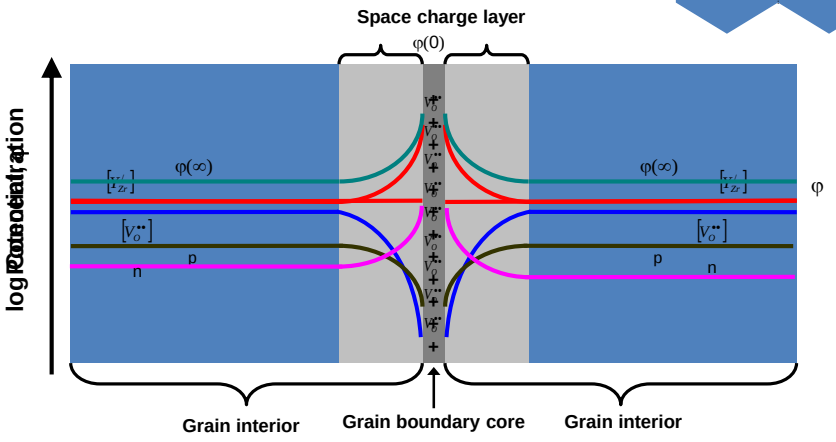

Dopant segregation and space charge effects in proton-conducting $BaZrO_3$ perovskites

M. Shirpour…J. Maier,
J. Phys. Chem. C 2012, 116, 2453–2461

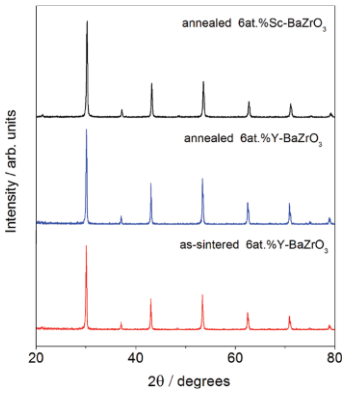

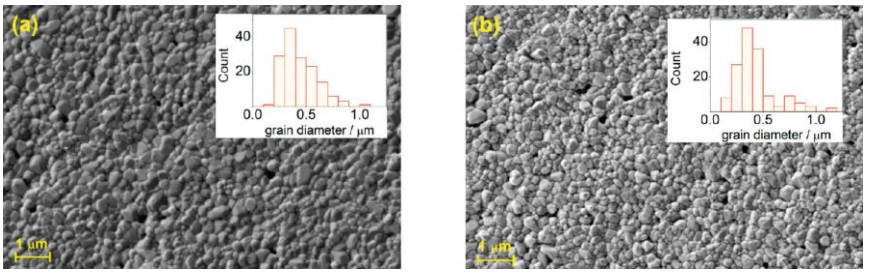

SEM image and grain size distribution of 6 at %Y-$BaZrO_3$ (a) as-sintered SPS sample and (b) annealed for 20 h at 1700 C in air.

Dopant segregation and space charge effects in proton-conducting $BaZrO_3$ perovskites

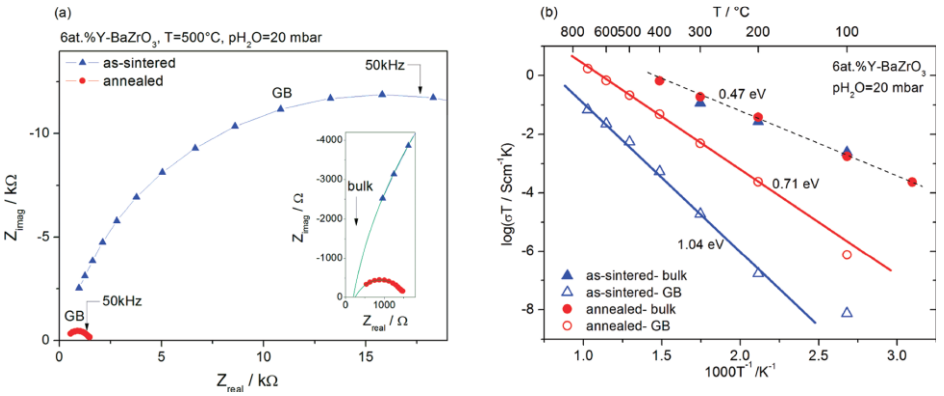

(a) AC impedance spectra at 500 °C and (b) Arrhenius plots of as-sintered and annealed 6 at% Y-doped $BaZrO_3$ in wet atmosphere (pH_2O= 20 mbar)

Dopant segregation and space charge effects in proton-conducting $BaZrO_3$ perovskites

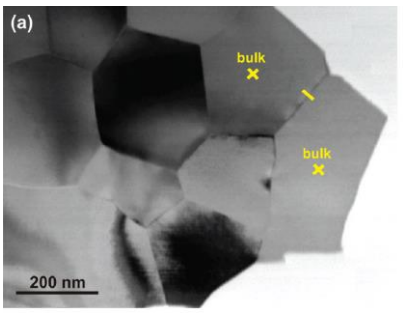

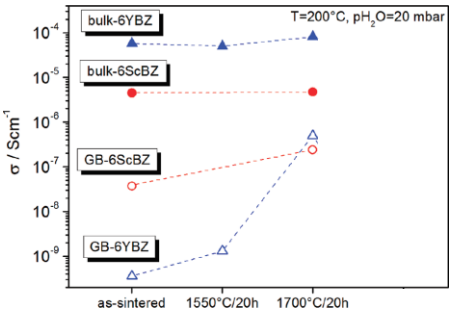

Bulk and grain boundary conductivities of 6 at% Y- and Sc- doped $BaZrO_3$ under different annealing condition

Dopant segregation and space charge effects in proton-conducting $BaZrO_3$ perovskites

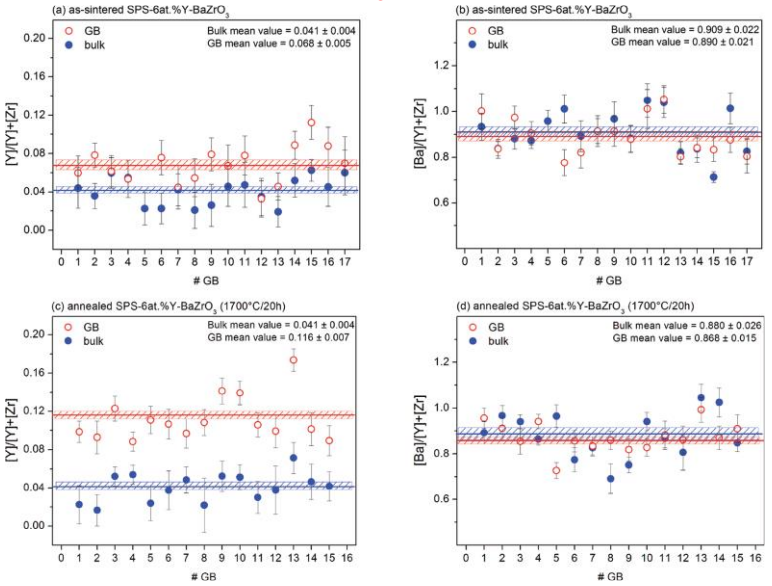

Y and Ba concentration of the GB region compared with the bulk of (a,b) as-sintered and (c,d) annealed 6 at%Y-doped $BaZrO_3$.

12

Dopant segregation and space charge effects in proton-conducting $BaZrO_3$ perovskites

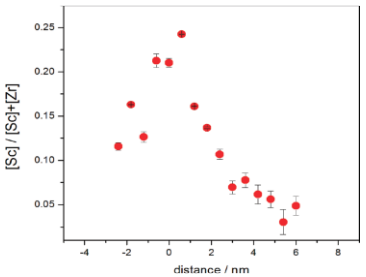

The local GB composition by transmission electron microscopy with spatially resolved energy dispersive X-ray analysis lines can across a GB of annealed SPS-6 at% Sc-doped $BaZrO_3$

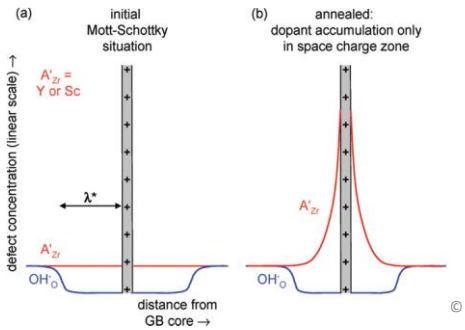

Schematic drawing of dopant (A'_{Zr}) and proton concentrations ($OH_O^{\cdot}$) at a grain boundary. (a) As-prepared sample (Mott-Schottky situation: constant dopant concentration, core charge exclusively compensated by proton depletion). (b) After annealing: case of dopant accumulation in the space charge zone (contributing to compensation of core charge) but not in the GB core.

13

Size Effect on Transport Phenomena

- *Depletion of space charges (nanocrystalline $SrTiO_2$)*

Electrical conduction in bi-crystal with a single interface – role of interfaces and boundaries

Fe doped $SrTiO_3$ - bicrystal

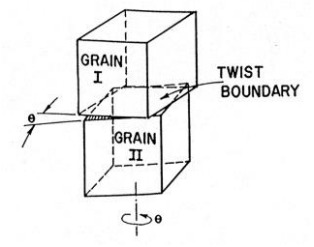

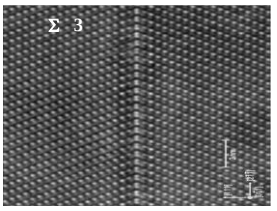

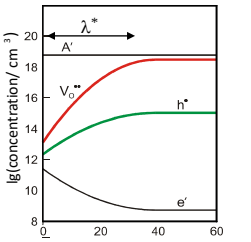

Distance from grain boundary/nm

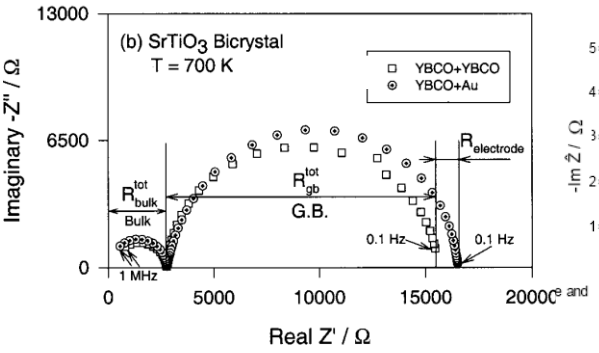

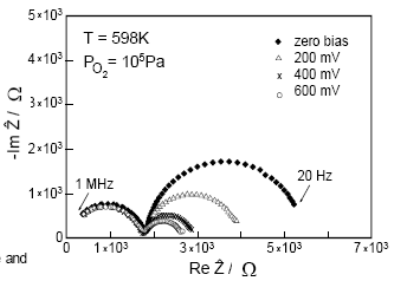

Size effect on grain boundary resistance

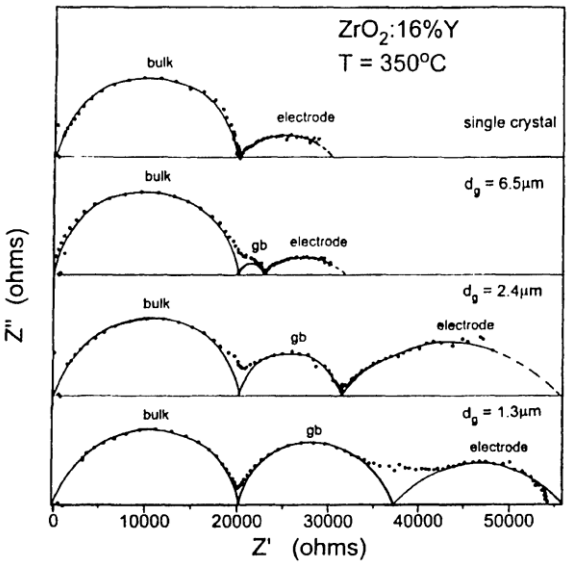

Complex impedance spectra obtained for (a) single crystal and microcrystalline YSZ bulk specimens (*H.L. Tuller, Solid State Ionics 131 (2000) 143-157)*.

16

Size effect on conductivity of TiO_2

$$Ti_{Ti}^{x} + 2O_O^x \leftrightarrow Ti_i^{\cdots\cdot} + 4e' + O_2(g)$$

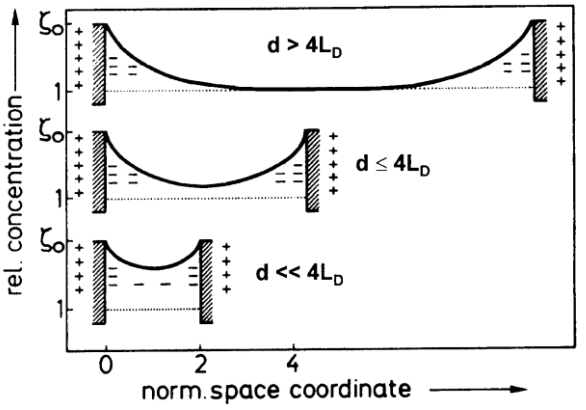

Defect profiles in structures with dimension, d. The build defect concentration is not reached when d **<<** 4L, where L, is the Debye length

J. Maier, Solid State Ionics 23 (1987) 59; C D. Terwilliger and Y.-M. Chiang *J, Am. Caam. Sac.,* 78, *2045-55 (1995)*

18

Ionic conduction in CaF_2/BaF_2 layers

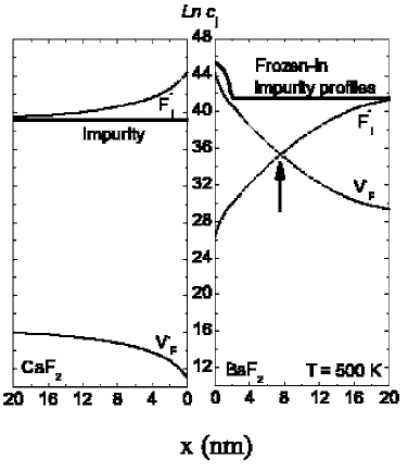

Defect concentration profiles at T=500 K for CaF_2/BaF_2 layers. Mott-Schottky profiles with frozen-in impurity (concentration of impurity varies) are shown for BaF_2, while Gouy-Chapman profiles (concentration of impurity remains constant) for CaF_2.

Ion conduction across nanosized CaF_2/BaF_2 multilayer heterostructures; X.X. Guo…J. Maier, Appl. Phys. Lett. 91, 103102 (2007)

19

Artificial mesoscopic ion conductors: accumulation situation

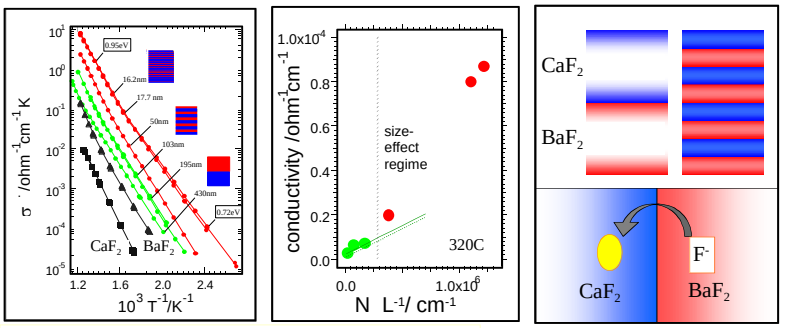

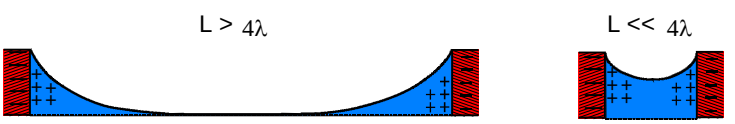

N. Sata, K. Eberman, K. Eberl and J. Maier, *Nature* 408 (2000) 946

20

Nanocrystalline $SrTiO_3$

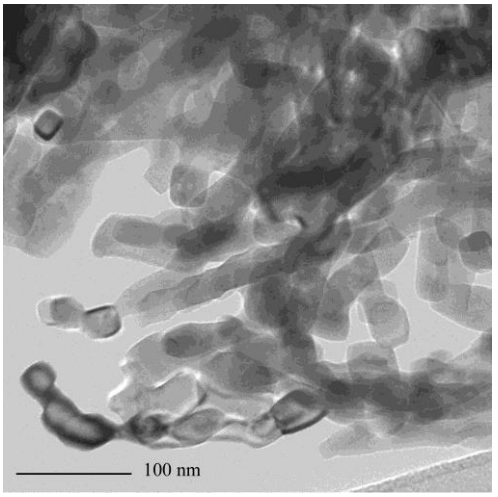

TEM image of $SrTiO_3$ nanopowder

Co-precipitation method

Calcination at 1275 K for 1 hr

Average grain size: (30 ± 5 nm)

XRD - confirmed single phase formation

Sr/Ti = 1.004

Total amount of electrochemically active impurities present (ICP):

~ 100 ppm (iron)

Nanoceramic $SrTiO_3$

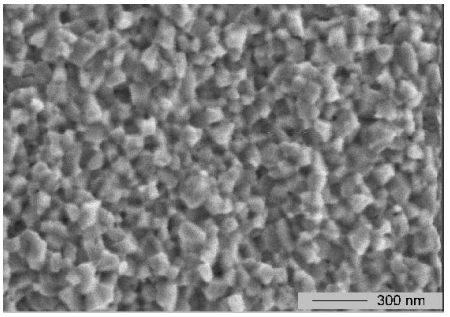

FESEM image - fractured surface,

Density : 93 %, Average grain size: 80 nm

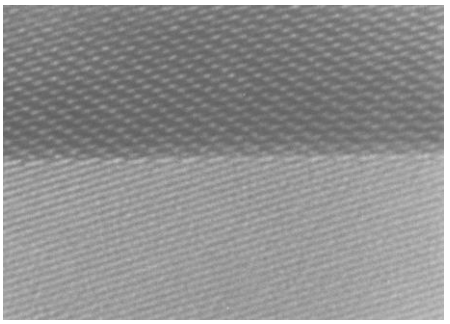

Edge-on view of grain boundary - HRTEM

No amorphous phase - during sintering

Impedance spectra of nanocrystalline $SrTiO_3$

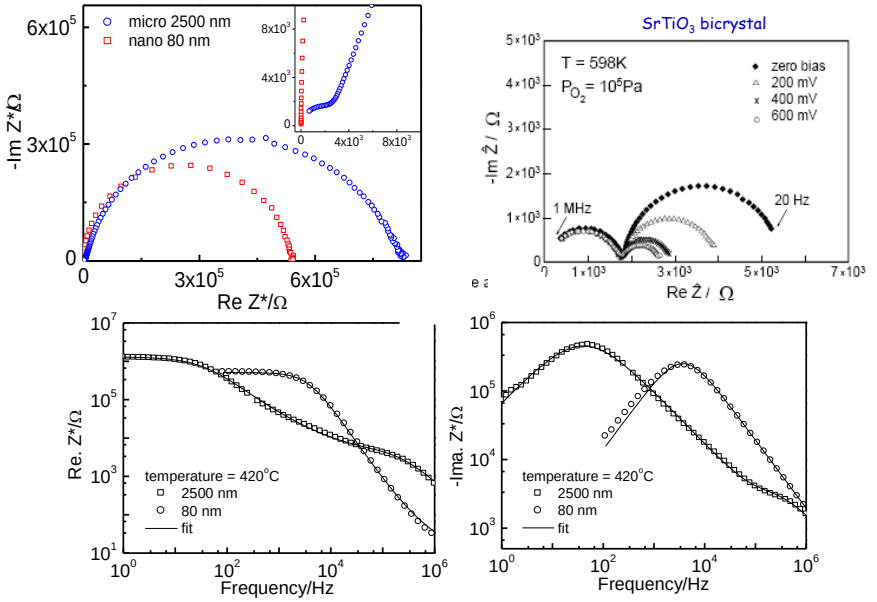

Mesoscopic (depletion) situation

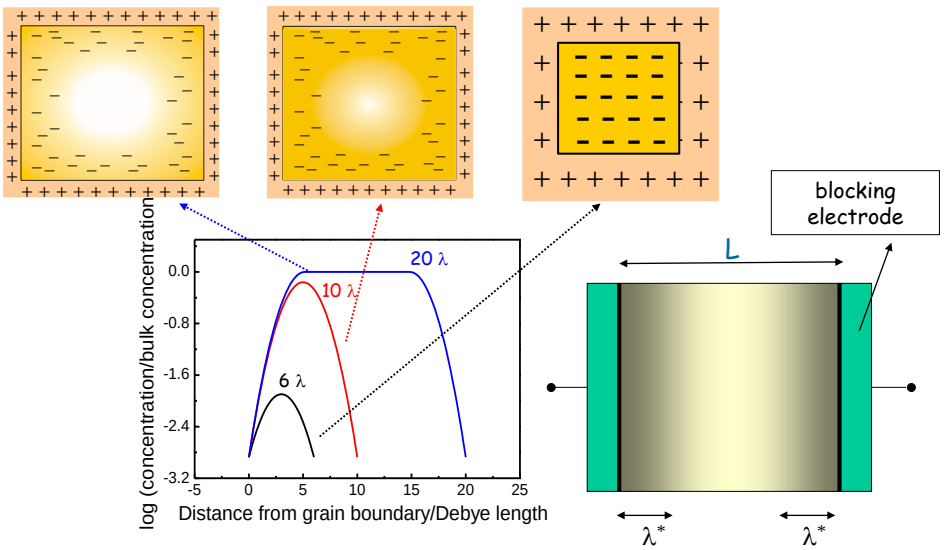

P. Balaya, J. Jamnik, J. Fleig & J. Maier, *Appl. Phys. Lett.*, 86 (2006) 062109;
P. Balaya, J. Jamnik, J. Fleig & J. Maier *J. Electrochem. Soc.* 154 (2007) P69

Thermodynamics at Nanosize

Relationship between melting temperature and particle diameter of gold nanoparticles

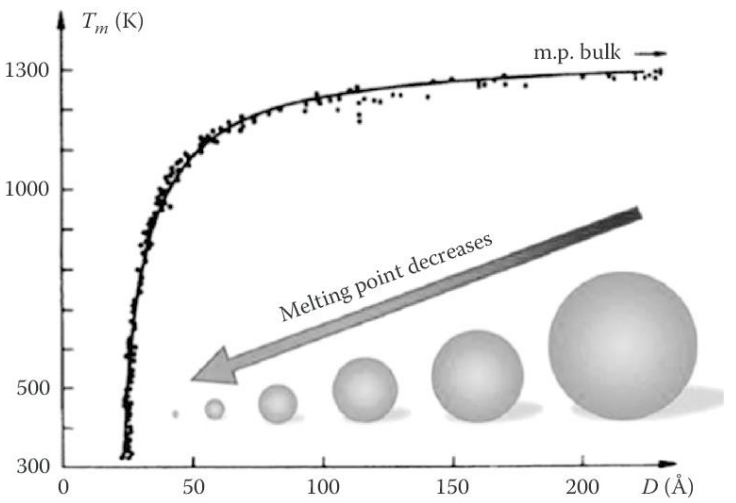

C. Yang et al., J. Mater. Chem. C, 1 (2013) 4052

Titanium dioxide (TiO_2)

Anatase
(thermodynamically less stable)

Rutile
(thermodynamically more stable)

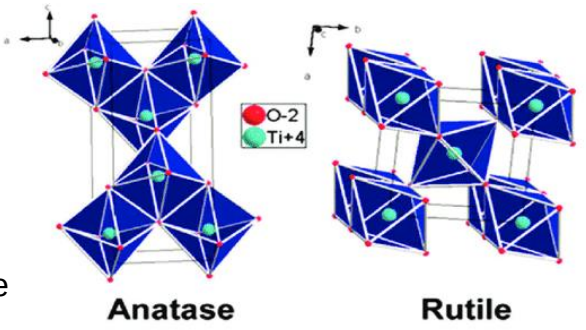

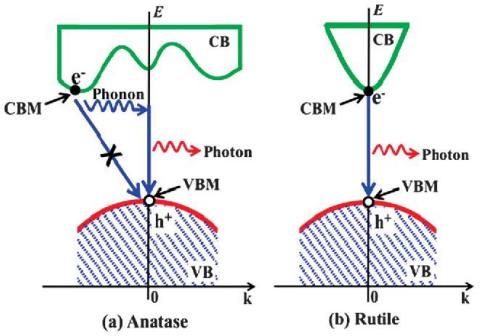

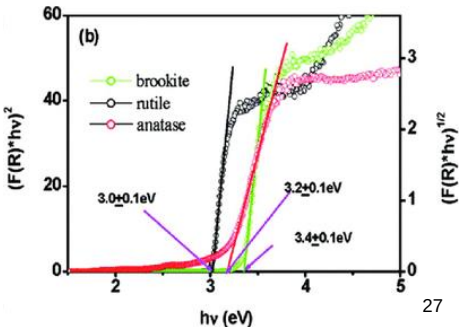

27

Energetics of nanocrystalline titania

$$\mu_{MX}^{nano} = \mu_{MX}^{\infty} + 2\frac{\bar{\gamma}}{\bar{r}}V_m$$

TiO_2 **nano-rutile** , $Na_2Ti_6O_{13}$, Au	β" - Al_2O_3 (Na_2O)	TiO_2 rutile (2 μ), $Na_2Ti_6O_{13}$, Au
Working electrode	Electrolyte	Reference electrode

Electrode reaction: $Na_2Ti_6O_{13} \rightleftharpoons 2Na^+ + 2\,e^- + 1/2\,O_2 + 6\,TiO_2$

Cell reaction: TiO_2 (nano-rutile) → TiO_2 (micro-rutile)

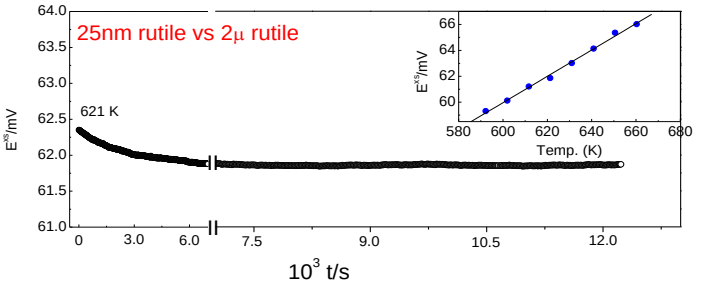

28

Energetics of nanocrystalline titania

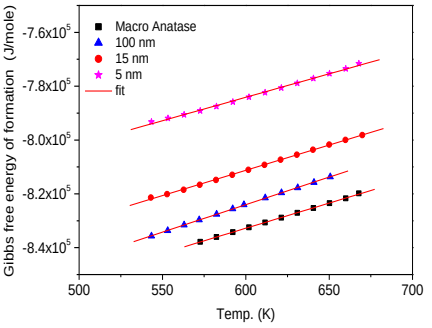

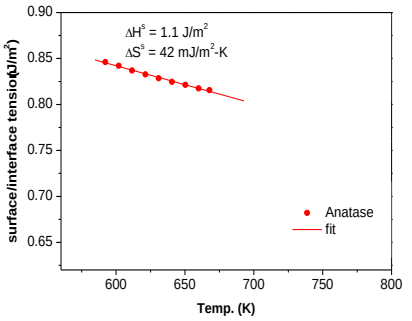

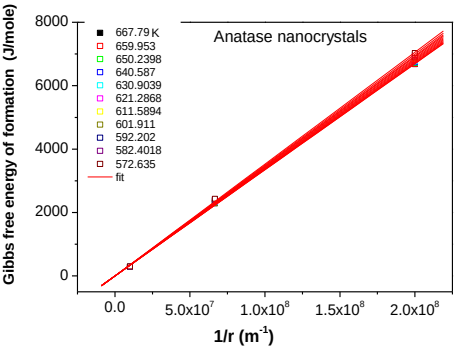

$$\Delta G^{xs} = \frac{2\bar{\gamma}}{\bar{r}} V_M = -nFE^{xs}$$

$$\bar{r} \sim 1nm, \bar{\gamma} \sim 1Jm^{-2}$$

$E^{xs} \sim 100$ mV

P. Balaya and J. Maier, *Phys. Chem. Chem Phys. 12 (2010) 215.*

29